Cellulose Acetate/Multiwalled Carbon Nanotube Nanocomposites with Improved Mechanical, Thermal, and Electrical Properties

Meilu Li, Il-Hwan Kim, Young Gyu Jeong

School of Advanced Materials and System Engineering, Kumoh National Institute of Technology, Gumi 730-701, Republic of Korea

Received 26 November 2009; accepted 10 April 2010
DOI 10.1002/app.32591
Published online 22 June 2010 in Wiley InterScience (www.interscience.wiley.com).

ABSTRACT: Cellulose acetate (CA)-based nanocomposites with various contents of neat multiwalled carbon nanotube (MWCNT) or acid-treated one (MWCNT-COOH) are prepared via melt-compounding method and investigated their morphology, thermal stability, mechanical, and electrical properties. SEM microphotographs reveal that MWCNT-COOHs are dispersed uniformly in the CA matrix, compared with neat MWCNTs. FTIR spectra support that there exists a specific interaction between carboxyl groups of MWCNT-COOHs and ester groups of CA, indicating good interfacial adhesion between MWCNT-COOHs and CA matrix. Accordingly, thermal stability and dynamic mechanical properties of CA/MWCNT-COOH nanocomposites were higher than those of CA/MWCNT composites. On the contrary, electrical volume resistivities of CA/MWCNT-COOH nanocomposites are found to be somewhat higher than those of CA/MWCNT composites, which is because of the deterioration of graphene structures for MWCNT-COOHs and the good dispersion of MWCNT-COOHs in the CA matrix.
 J Appl Polym Sci 118: 2475–2481, 2010

Key words: cellulose acetate; multiwalled carbon nanotube; nanocomposites; mechanical property; electrical resistivity; thermal stability

INTRODUCTION

In recent years, much attention has been paid to renewable natural polymers because the energy crisis and environmental problems becomes severe.[1] Accordingly, eco-friendly biodegradable polymers from renewable resources have attracted great attention with expertise in diverse areas. As a renewable source-based biodegradable polymer, cellulose acetate (CA) is a kind of thermoplastic material produced by the esterification of naturally abundant cellulose materials such as cotton, wood pulp, sugarcane, and recycled paper.[2–5] Owing to potential compostibility, excellent optical and mechanical properties, CA has been used for the applications in diverse areas such as fibers, films, laminates, adhesives, coatings, plastic products, etc.[6–8]

Polymer nanocomposites are commonly defined as the combination of a polymer matrix and additives that have at least one dimension in the nanometer range.[9,10] The additives can be one-dimensional (nanotubes and fibers),[11–15] two-dimensional (clay and graphite),[16–20] or three-dimensional (spherical particles).[21–23] Adding such additives to polymers can effectively enhance the properties of composites such as strength, modulus, and thermal stability. Carbon nanotube (CNT) is one of the nanoadditives and considered as the ideal reinforcing nanofiller for polymer matrix, because of its unique mechanical property, thermal stability, high aspect ratio, and electrical conductivity.[24–27] However, their nonreactive surface and strong aggregative properties have limited the effectiveness of CNT with the polymer matrix they reinforce. If the unique multifunctional properties of CNT are to be utilized for effective reinforcement, the good dispersion of CNTs as well as the good interfacial adhesion between CNTs and the polymer matrix is a prerequisite.[14,28–32] So far, various polymer/CNT nanocomposites have been prepared. Nevertheless, to our knowledge, there have been no reports on nanocomposites based on CA and CNT.

In this study, our objective focuses on testing the hypothesis that CNT nanofiller can improve the physical properties of CA polymer and the surface modification of CNT can provide a route to enhance adhesion between CNTs and CA matrix in nanocomposites. Accordingly, we have prepared CA/CNT nanocomposites by melt-compounding of CA with neat multiwalled carbon nanotube (MWCNT) or acid-treated one (MWCNT-COOH), and investigated their thermal, mechanical, and electrical performances in conjunction with morphological features.

Correspondence to: Y. G. Jeong (ygjeong@kumoh.ac.kr).

EXPERIMENTAL

Materials

The CA in a powdery form (acetyl content of 39.7 wt %, degree of substitution of 2.45, and $\overline{M}_n \sim$ 50,000 g/mol) was supplied from Sigma-Aldrich Co. (St. Louis, MO). Neat MWCNT (diameter of 10–15 nm, length of 10 $\sim$ 20 μm, and purity of $\sim$ 95 wt %) was purchased from Hanwha Nanotech Co. (Seoul, Korea). Sulfuric acid (95%) and nitric acid (60%) for the acid treatment of MWCNT were purchased from Junsei Chemical Co. (Tokyo, Japan).

Preparation of MWCNT-COOH

Neat MWCNT was first refluxed in a mixture of sulfuric acid (95%)/nitric acid (60%) (3 : 1 by mol ratio) at 120°C for 2 h. After cooling to the room temperature, the mixed solution was diluted with distilled water and filtered through a membrane with a pore size of 0.22 μm, which was repeated several times until the pH approached 7.0. In the end, the filtrated solid was dried in a vacuum oven at 120°C for 24 h to obtain acid-treated MWCNT (MWCNT-COOH).

Preparation of CA/MWCNT-COOH nanocomposites

Nanocomposites based on CA and MWCNT-COOH were prepared by a melt-compounding method. Before melt-compounding, all the components were dried in vacuum at 80°C for 24 h. At first, solid state mixtures of CA and MWCNT-COOH with various ratios were mixed mechanically for 3 min. The solid mixtures were then melt-extruded through a corrotating twin-screw extruder (BK-11, Bowtek Com.) with screw length of 440 mm and screw diameter of 11 mm. The temperature profile of extruder from Zone 1 to Zone 6 was set to be 235, 240, 245, 250, 260, and 260°C. The screw speed was fixed at 180 rpm. The extruded strands were cooled into water bath, chopped into pellets, and dried under vacuum at 80°C for 24 h. For structural characterization and physical properties analyzes of CA-based nanocomposites with various contents of MWCNT or MWCNT-COOH, the melt-quenched films of 0.20 mm thickness were prepared by compression-molding in a hot-plate at 250°C and 18 MPa for 4 min, quenching into cold water, and dried in the vacuum oven at 60°C overnight. For comparison, CA/MWCNT composite films were prepared in the same way.

Characterization of CA/MWCNT-COOH nanocomposites

Chemical structures of nanocomposite films including neat MWCNT or MWCNT-COOH were characterized by using a Fourier Transform Infrared (FTIR) spectrometer (Tensor 27, Bruker) in an attenuated total reflectance (ATR) mode with a ZnSe crystal.

Dispersion state of CNTs in the nanocomposites was examined by a scanning electron microscope (SEM, JEOL-JSM 6380). The samples for SEM images were prepared by fracturing the nanocomposite films in liquid nitrogen and then sputtering the fractured surfaces with gold.

Dynamic mechanical properties of the nanocomposite films with dimensions of 35 × 5 × 0.2 mm^3 were examined on a dynamic mechanical analyzer (DMA, TA Q800) under the tensile mode from 0 to 250°C at a heating rate of 2°C/min and a frequency of 1 Hz.

Thermal stability of the nanocomposites was investigated by using a thermogravimetric analyzer (TGA, TA Q500) under the nitrogen gas at a heating rate of 20°C/min.

Electrical properties of the nanocomposites were evaluated by measuring electrical surface resistivity with an electrometer high resistance meter with a resistivity test fixture (6517A, Keithley Instruments, Inc., Cleveland, USA).

RESULTS AND DISCUSSION

Structural and morphological characterization of nanocomposites

The interfacial adhesion of CNT and CA matrix in the nanocomposites was identified by using FTIR spectroscopy. Figure 1 shows FTIR spectra of pure CA and its nanocomposites reinforced with neat MWCNT and MWCNT-COOH of 1.0 wt %. The pure CA exhibited a strong carbonyl (C=O) stretching band at $\sim$ 1738 cm^{-1} becasue of the existence of acetate groups. FTIR spectra of the nanocomposites were almost identical with that of the pure CA, except for the band position of carbonyl groups. For pure CA and CA/MWCNT nanocomposite, the C=O stretching band was detected at $\sim$ 1738 cm^{-1}, whereas it appeared at $\sim$ 1734 cm^{-1} for CA/MWCNT-COOH nanocomposite. Therefore, it is believed that the shift of the C=O stretching band to lower wavenumber is owing to the specific interaction between carboxylic acid groups of MWCNT-COOHs and carbonyl groups of CA matrix, as can be seen in Figure 2.

To characterize the dispersion state of CNTs in the CA matrix, fractured surfaces of nanocomposite films were examined by using SEM, as shown in Figure 3. The fractured surface of the pure CA film is quite even and smooth, exhibiting a typical brittle failure [Fig. 3(A)]. At low CNT loadings of 0.1 and 1.0 wt %, MWCNTs or MWCNT-COOHs are dispersed well in the CA matrix [Fig. 3(B,C,E,F). However, at high CNT loading of 7.0 wt %, MWCNTs or

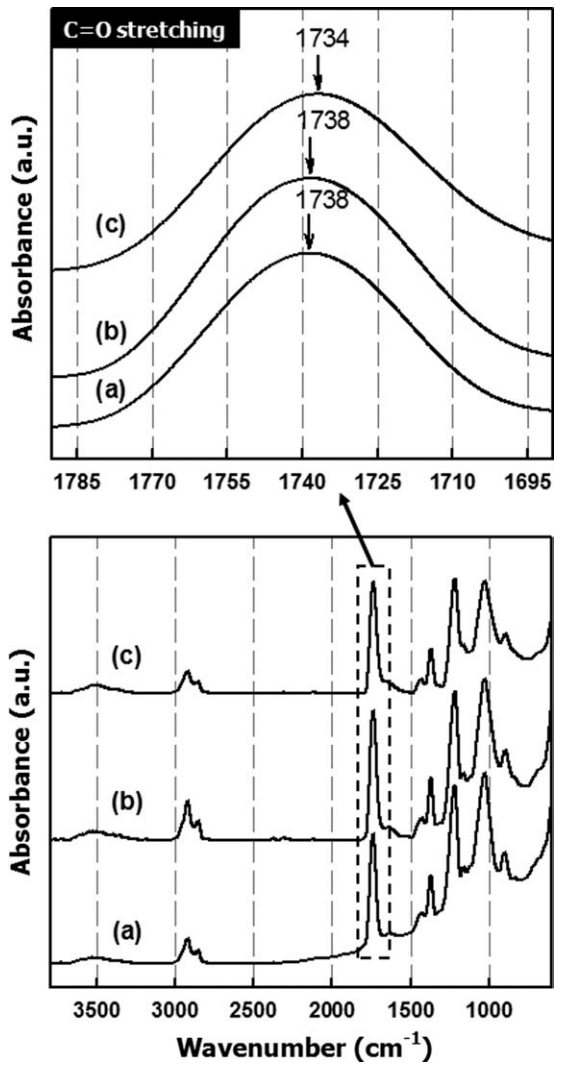

Figure 1 FTIR spectra of (a) CA homopolymer, (b) nanocomposite with 1.0 wt % MWCNT, and (c) nanocomposite with 1.0 wt % MWCNT-COOH.

MWCNT-COOHs are found to form their aggregates to some extent in the matrix [Fig. 3(D,G)]. It means that even MWCNT-COOHs are not dispersed well in the CA matrix at high CNT contents, because of the van der Waals interaction between neighboring CNTs. It is noteworthy that, for CA/MWCNT nanocomposites, some MWCNTs are pulled out from the CA matrix [Fig. 3(D)], which is because of the relatively weak interfacial adhesion between neat MWCNTs and the CA matrix.

Mechanical properties of nanocomposites

Figure 4 displays the changes of dynamic storage moduli of the nanocomposites with various MWCNT or MWCNT-COOH loadings as a function of temperature. With increasing the temperature, the storage moduli decreased slightly at the glassy region and then decreased abruptly at the glass transition region. When the storage moduli of the nanocomposites at room temperature were plotted as a function of CNT content, as shown in Figure 5, it was revealed that the storage moduli of CA/MWCNT-COOH nanocomposites were somewhat higher than those of counterparts at the same CNT content. This result is caused by the fact that CA/MWCNT-COOH nanocomposites have better interfacial adhesion owing to the existence of specific interaction between MWCNT-COOHs and the CA matrix. Therefore, the external stress is effectively transferred from the CA matrix to reinforcing CNTs through the better bonded interfaces in CA/MWCNT-COOH nanocomposites. As noted above, the interfacial adhesion between CNTs and the matrix is one of crucial factors affecting on mechanical properties of the composites.[14,28–32] In fact, it has been reported that, functionalized MWCNT have a greater affinity to the polymer matrix, resulting in a significant improvement on the storage modulus of the polymer matrix.[33,34] For CA/MWCNT-COOH nanocomposites, the storage moduli increased with the CNT content up to ~ 3.0 wt % and then decreased at higher CNT content above 3.0 wt %. In cases of CA/MWCNT nanocomposites, the storage moduli increased up to ~ 1.0 wt % and then remained unchanged at higher CNT content. The decreased storage moduli at higher CNT contents for both nanocomposites are attributed to the

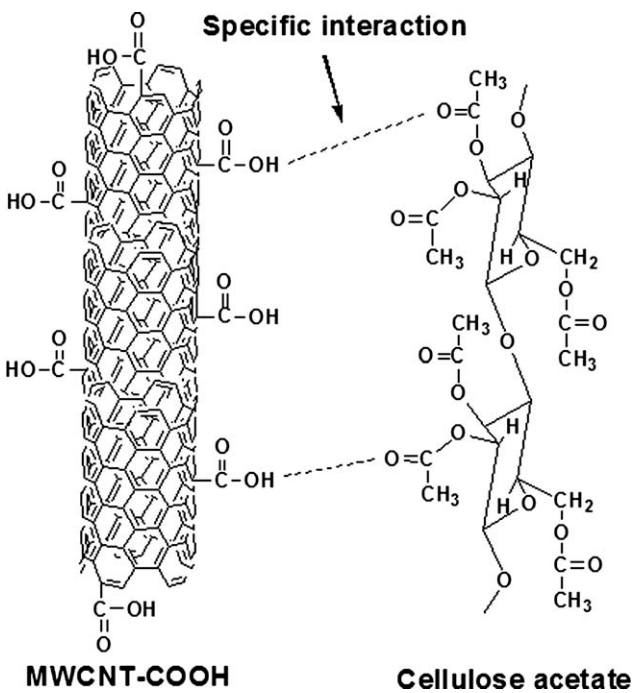

Figure 2 Schematic diagram showing a specific interaction between MWCNT-COOH and CA matrix.

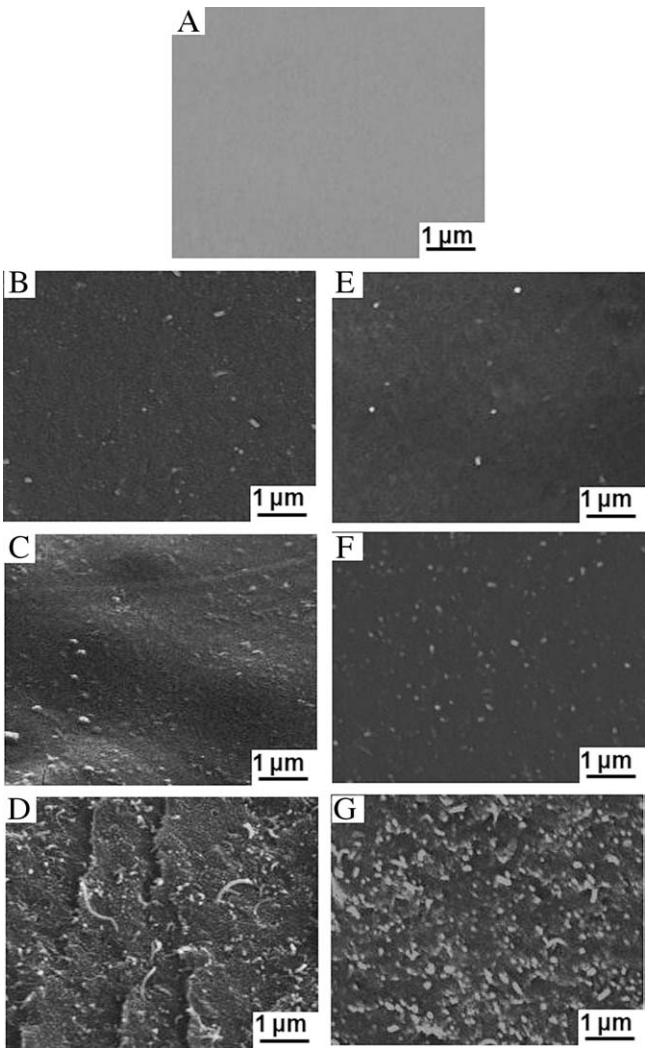

Figure 3 SEM images of cryogenically fractured surfaces of CA homopolymer and its nanocomposites with various CNT contents: (A) CA homopolymer; (B) 0.1 wt % MWCNT; (C) 1.0 wt % MWCNT; (D) 7.0 wt % MWCNT; (E) 0.1 wt % MWCNT-COOH; (F) 1.0 wt % MWCNT-COOH; (G) 7.0 wt % MWCNT-COOH.

aggregation of a large number of CNT in the CA matrix, as described above based on SEM images.

Based on the assumption that MWCNTs are randomly distributed in the CA matrix and perfectly bonded with the matrix, the storage moduli, $E_{composite}$, of nanocomposites can be predicted according to the following equation[35]

$$E_{composite} = \left[\frac{3}{8}\frac{1+2\left(\frac{l_{MWCNT}}{d_{MWCNT}}\right)\eta_L V_{MWCNT}}{1-\eta_L V_{MWCNT}} + \frac{5}{8}\frac{1+2\eta_T V_{MWCNT}}{1-\eta_T V_{MWCNT}}\right] E_{CA} \quad (1)$$

$$\eta_L = \frac{(E_{MWCNT}/E_{CA})-1}{(E_{MWCNT}/E_{CA})+2(l_{MWCNT}/d_{MWCNT})}$$

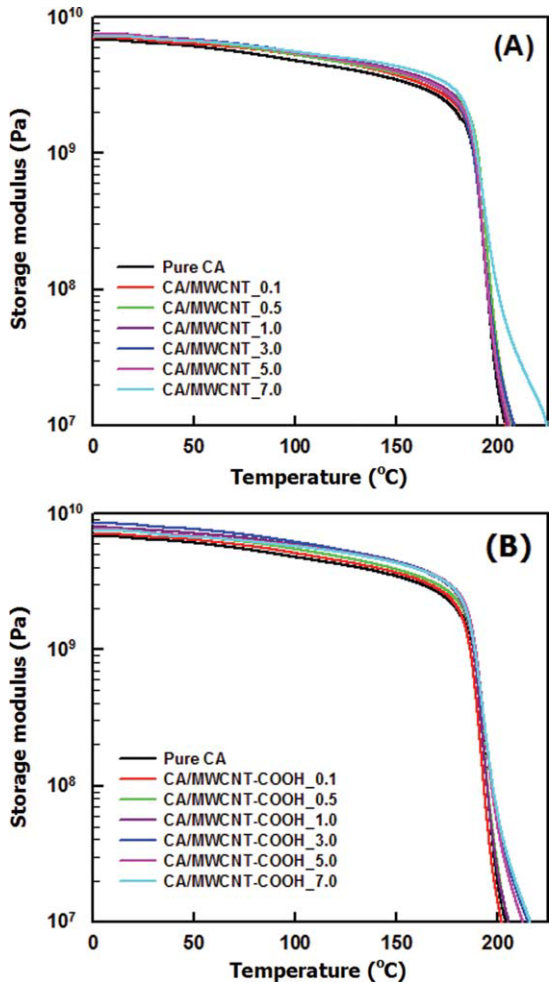

Figure 4 Dynamic storage moduli of (A) CA/MWCNT and (B) CA/MWCNT-COOH nanocomposites as a function of temperature [Color figure can be viewed in the online issue, which is available at www.interscience.wiley.com.]

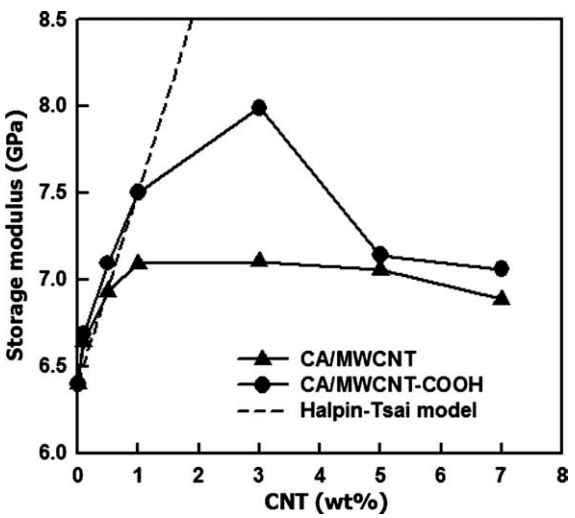

Figure 5 Comparison of experimental storage moduli at 35°C for CA/MWCNT and CA/MWCNT-COOH nanocomposites with the moduli predicted by Halpin-Tsai model expressed as eq. (1).

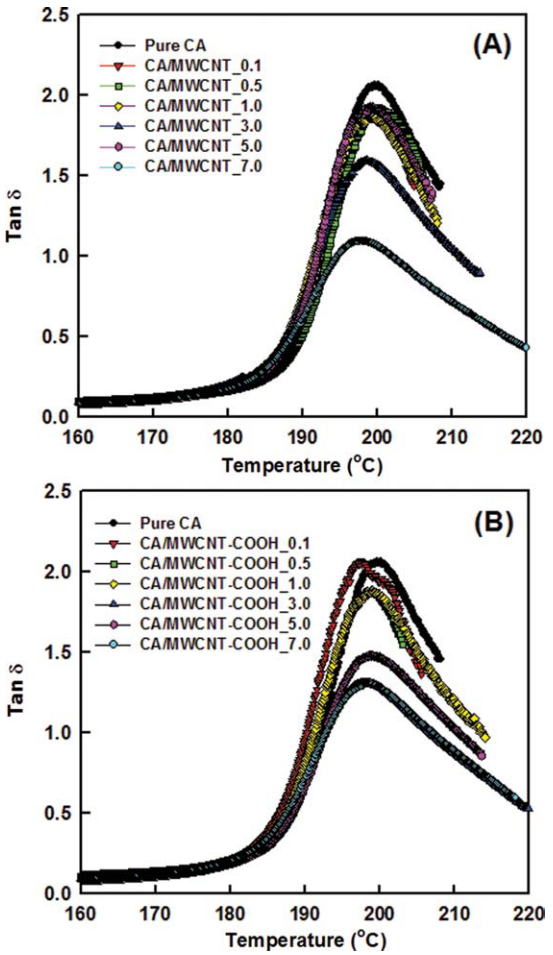

Figure 6 Tan δ of (A) CA/MWCNT and (B) CA/MWCNT-COOH nanocomposites as a function of temperature [Color figure can be viewed in the online issue, which is available at www.interscience.wiley.com.]

$$\eta_T = \frac{(E_{MWCNT}/E_{CA}) - 1}{(E_{MWCNT}/E_{CA}) + 2}$$

$$V_{MWCNT} = \left[1 + \left(\frac{\rho_{MWCNT}}{\rho_{CA}}\right)\left(\frac{1 - m_{MWCNT}}{m_{MWCNT}}\right)\right]^{-1}$$

where E_{MWCNT} and E_{CA} are storage moduli of MWCNT (400 GPa) and CA (6.4 GPa), respectively. l_{MWCNT} and d_{MWCNT} are length (15 μm) and diameter (12.5 nm) of MWCNT used in this study, respectively. V_{MWCNT}, the volume fraction of MWCNT in the nanocomposites, can be calculated from the MWCNT weight fraction (m_{MWCNT}), MWCNT density ($\rho_{MWCNT} \sim 1.8$ g/cm^3), and amorphous CA density ($\rho_{CA} \sim 1.28$ g/cm^3). The predicted moduli estimated from eq. (1) are represented as a dotted line, in Figure 5. It was found that the experimental storage moduli of the nanocomposites were almost similar with the predicted values at lower CNT content less than 1.0 wt %, but they were far lower than the calculated values at higher CNT content above 1.0 wt %. It indicates that the mechanical reinforcing effect of MWCNT-COOH is dominant at lower CNT content, because of the good dispersion and interfacial adhesion of MWCNT-COOHs in the CA matrix, whereas the aggregation effect of MWCNT-COOHs is prevalent at higher CNT contents owing to the van der Waals attraction between CNTs and their high surface area.

Tan δ versus temperature data for nanocomposites can be seen in Figure 6. It was revealed that the peak position of tan δ, which corresponds to the glass transition temperature, remained constant by adding CNT within the experimental error, whereas the peak width slightly increased, dominantly for CA/MWCNT-COOH nanocomposites. It is considered that the noticeable peak broadening for CA/MWCNT-COOH nanocomposites stems from the existence of better interfacial affinity between carboxylic acid groups of MWCNT-COOH and the acetyl groups of CA matrix, as proved by the FTIR data.

Thermal degradation behavior of nanocomposites

TGA thermograms of CA/MWCNT and CA/MWCNT-COOH nanocomposites with various CNT contents were shown in Figure 7. Thermal degradation profiles revealed that thermal stability of the CA/MWCNT-COOH nanocomposites was improved with the increment of MWCNT-COOH content. However, thermal degradation behavior of CA/MWCNT nanocomposites was found to be almost identical to that of pure CA, irrespective of the MWCNT content. Only the residue after the dominant thermal degradation at higher temperatures was increased with the initial CNT content in the nanocomposites. For the quantitative comparison of thermal stabilities between CA/MWCNT-COOH and CA/MWCNT composites, the thermal degradation temperatures of 10% and 50% weight losses ($T_{10\%}$ and $T_{50\%}$) were evaluated from the TGA thermograms of Figure 7 and summarized in Table I. $T_{10\%}$ and $T_{50\%}$ of CA homopolymer was determined to be about 361 and 388°C, respectively. In cases of CA/MWCNT composites, the thermal degradation temperatures are almost same with those of CA homopolymer, regardless of MWCNT content, within the experimental error. On the contrary, thermal degradation temperatures of CA/MWCNT-COOH nanocomposites increased with the MWCNT-COOH content up to ~ 1.0 wt % and then decreased slightly at higher MWCNT-COOH contents. For instance, $T_{10\%}$ and $T_{50\%}$ of the nanocomposite with 1.0 wt % MWCNT-COOH were between ~ 365 and ~ 390°C, respectively, which were approximately 2 ~ 4°C higher than those of CA homopolymer. However, the decreased thermal stability of the nanocomposites with higher MWCNT-COOH

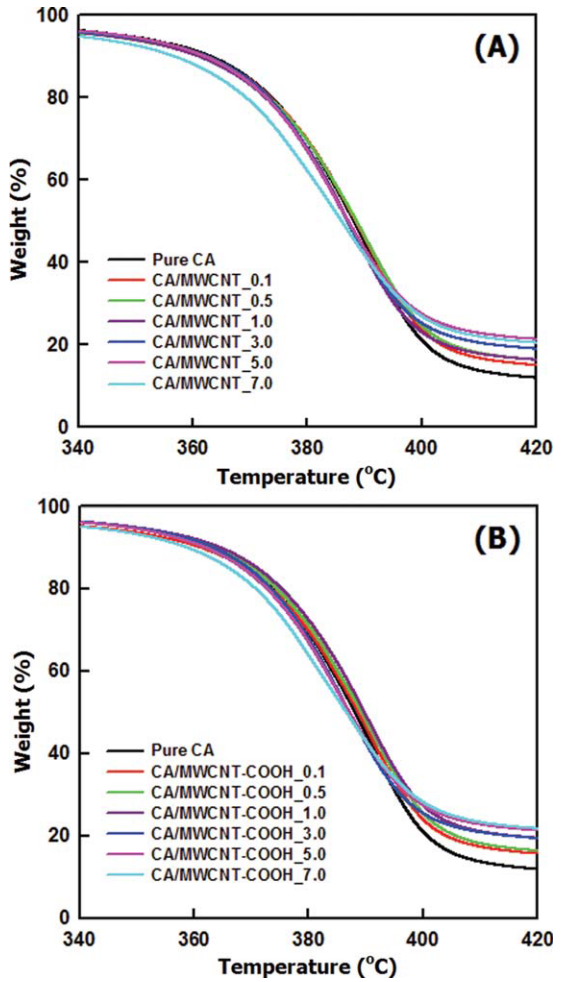

Figure 7 TGA thermograms of (A) CA/MWCNT and (B) CA/MWCNT-COOH nanocomposites [Color figure can be viewed in the online issue, which is available at www.interscience.wiley.com.]

contents above 3.0 wt % is because of the aggregation of MWCNT-COOHs in the matrix. Overall, it is believed that slightly improved thermal stability of CA/MWCNT-COOH nanocomposites originates from the fact that MWCNT-COOHs, which were dispersed homogeneously in the CA matrix, serve as the retarding agents for thermal degradation of the CA matrix.

Electrical properties of nanocomposites

Electrical properties of CA/MWCNT and CA/MWCNT-COOH nanocomposite films were evaluated by measuring electrical volume resistivities of nanocomposite as a function of CNT content, as shown in Figure 8. Electrical resistivity of the pure CA film was measured to be about $\sim 10^{16}$ Ω cm. In cases of nanocomposites, the electrical resistivities remained unchanged up to ~ 1.0 wt % CNT and decreased substantially at the higher CNT content above ~ 1.0 wt %. This result illustrated that electrical conduction path of CNT in the CA matrix was attained at the higher CNT content above ~ 1.0 wt %. However, compared with CA/MWCNT nanocomposites, CA/MWCNT-COOH nanocomposites exhibited a lower decrement of electrical resistivity, which could be caused by following two reasons. First, by the acid treatment, graphene structure of MWCNT-COOH was partially damaged. It has been known that this damage could be ascribed to the rigorous conditions used for the acid treatment of MWCNT. Second, MWCNT-COOH was well dispersed in the CA matrix, compared with neat MWCNT, as discussed above. It means that higher content of MWCNT-COOH is required to reach electrical percolation threshold.

TABLE I
Thermal Degradation Temperatures ($T_{10\%}$ and $T_{50\%}$) of 10 and 50% Weight Loss for CA Homopolymer and its Nanocomposites with Various CNT Contents

Sample code	CNT (wt %)	$T_{10\%}$ (°C)	$T_{50\%}$ (°C)
CA	0.0	361.2	388.1
CA/MWCNT	0.1	361.2	388.3
	0.5	361.3	388.4
	1.0	361.2	387.1
	3.0	361.6	386.9
	5.0	361.6	387.0
	7.0	356.3	385.9
CA/MWCNT-COOH	0.1	361.1	388.6
	0.5	363.3	389.1
	1.0	364.5	389.8
	3.0	363.4	387.2
	5.0	362.0	387.1
	7.0	358.7	386.5

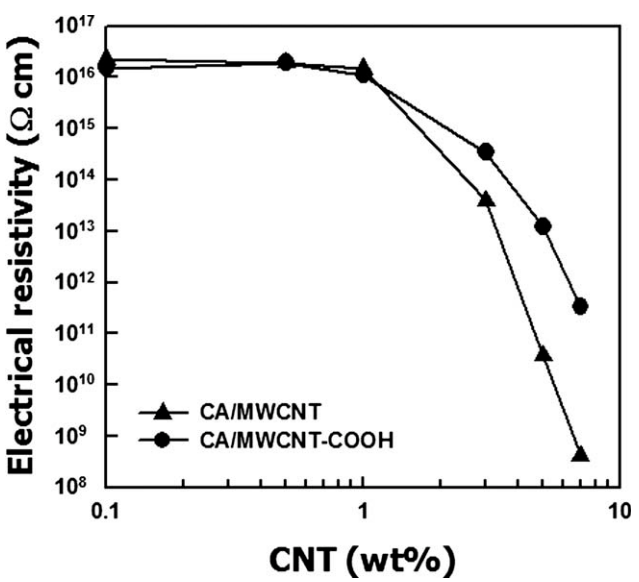

Figure 8 Electrical resistivities of (▲) CA/MWCNT and (●) CA/MWCNT-COOH nanocomposites as a function of CNT.

CONCLUSIONS

In this study, eco-friendly and melt-processible CA-based nanocomposites with various MWCNT contents were prepared via melt-compounding method and their morphology, thermal stability, mechanical and electrical properties were investigated. To enhance the dispersity of MWCNTs and the interfacial interaction between MWCNTs and the CA matrix, acid-treated MWCNT (MWCNT-COOH) were prepared. FTIR spectra of CA/MWCNT-COOH nanocomposites demonstrates that a specific interaction exists between carboxyl groups of MWCNT-COOHs and ester groups of CA, which leads to better interfacial adhesion between MWCNT-COOHs and CA matrix than CA/MWCNT nanocomposites. Accordingly, thermal stability and dynamic mechanical properties of CA/MWCNT-COOH nanocomposites were higher than those of CA-based nanocomposites including neat MWCNT. On the contrary, electrical volume resistivities of CA/MWCNT-COOH nanocomposites were found to be slightly higher than those of CA/MWCNT nanocomposites, which was attributed to the deterioration of graphene structures for MWCNT-COOH and as the good dispersion of MWCNT-COOHs in the CA matrix.

This paper was supported by Research Fund, Kumoh National Institute of Technology.

References

1. Scott, G. Polym Degrad Stab 2000, 68, 1.
2. Sassi, J. F.; Chanzy, H. Cellulose 1995, 2, 111.
3. Saka, S.; Ohmae, K. J Appl Polym Sci 1996, 62, 1003.
4. Tserki, V.; Zafeiropoulus, N. E.; Simon, F.; Panayiotou, C. Compos Part A-Appl Sci Manuf 2005, 36, 1110.
5. Filho, G. R.; Monteiro, D. S.; Meireles, C. D. S.; De Assuncao, R. M. N.; Cerqueira, D. A.; Barud, H. S.; Ribeiro, S. J. L.; Messadeq, Y. Carbohydr Polym 2008, 73, 74.
6. Edgar, K. J.; Buchanan, C. M.; Debenham, J. S.; Rundquist, P. A.; Seiler, B. D.; Shelton, M. C.; Tindall, D. Prog Polym Sci 2001, 26, 1605.
7. Biswas, A.; Shogren, R. L.; Willett, J. L. Biomacromolecules 2005, 6, 1843.
8. Barud, H. S.; de Araujo Jr., A. M.; Santos, D. B.; De Assuncao, R. M. N.; Meireles, C. S.; Cerqueira, D. A.; Filho, G. R.; Ribeiro, C. A.; Messadeq, Y.; Ribeiro, S. J. L. Thermochim Acta 2008, 471, 61.
9. Vaia, R. A.; Giannelis, E. P., Eds. Polymer Nanocomposites, American Chemical Society: Washington, 2001.
10. Sperling, L. H. Introduction to physical polymer science; Wiley: Hoboken, 2006.
11. Thostenson, E. T.; Ren, Z.; Chou, T.-W. Compos Sci Technol 2001, 61, 1899.
12. Lozano, K.; Barrera, E. V. J Appl Polym Sci 2001, 79, 125.
13. Lozano, K.; Bonilla-Rios, J.; Barrera, E. V. J Appl Polym Sci 2001, 80, 1162.
14. Breuer, O.; Sundararaj, U. Polym Compos 2004, 25, 630.
15. Zhang, H.; Wang, Z.; Wu, J.; Zhang, J.; He, J. Adv Mater 2007, 19, 698.
16. Giannelis, E. P. Adv Mater 1996, 8, 29.
17. Park, H.-M.; Liang, X.; Mohanty, A. K.; Misra, M.; Drzal, L. T. Macromolecules 2004, 37, 9076.
18. Ray, S. S.; Bousmina, M. Prog Mater Sci 2005, 50, 962.
19. Chen, B.; Evans, J. R. G.; Greenwell, H. C.; Boulet, P.; Conveney, P. V.; Bowden, A. A.; Whiting, A. Chem Soc Rev 2008, 37, 568.
20. Cote, L. J.; Cruz-Silva, R.; Huang, J. X. J Am Chem Soc 2009, 131, 11027.
21. Gangopadhyay, R.; De, A. Chem Mater 2000, 12, 608.
22. Sterescu, D. M.; Stamatialis, D. F.; Mendes, E.; Wubbenhorst, M.; Wessling, M. Macromolecules 2006, 39, 9234.
23. Zhou, T. H.; Ruan, W. H.; Rong, M. Z.; Zhang, M. Q.; Mai, Y. L. Adv Mater 2007, 19, 2667.
24. Treacy, M. M. J.; Ebbesen, T. W.; Gibson, J. M. Nature 1996, 381, 678.
25. Ebbesen, T. W.; Lezec, H. J.; Hiura, H.; Bennett, J. W.; Ghaemi, H. F.; Thio, T. Nature 1996, 382, 54.
26. Khare, R.; Bose, S. J Miner Mater Charac Eng 2005, 4, 31.
27. Uchida, T.; Kumar, S. J Appl Polym Sci 2005, 98, 985.
28. Coleman, J. N.; Khan, U.; Blau, W. J.; Gun'ko, Y. K. Carbon 2006, 44, 1624.
29. Coleman, J. N.; Khan, U.; Gun'ko, Y. K. Adv Mater 2006, 18, 689.
30. Xia, H.; Song, M.; Jin, J.; Chen, L. Macromol Chem Phys 2006, 207, 1945.
31. Villmow, T.; Potschke, P.; Pegel, S.; Haussler, L.; Kretzschmar, B. Polymer 2008, 49, 3500.
32. Yoon, J. T.; Jeong, Y. G.; Lee, S. C.; Min, B. G. Polym Adv Technol 2009, 20, 631.
33. Kim, J. A.; Seong, D. G.; Kang, T. J.; Youn, J. R. Carbon 2006, 44, 1898.
34. Yuen, S.-M.; Ma, C.-C. M.; Lin, Y.-Y.; Kuan, H.-C. Comps Sci Technol 2007, 67, 2564.
35. Mallick, P. K. Fiber-reinforced composites: material manufacturing and design; Marcel Dekker Inc.: New York, 1993.